

# Phase transitions in AI-human interaction networks: statistics, computation, and probabilistic modeling

Jackson George<sup>1,e</sup>, Zachariah Yusaf<sup>1,e</sup>, Stephanie Zoltick<sup>2,e</sup>, and Linh Huynh<sup>1,\*</sup>

<sup>1</sup>Dartmouth College, Department of Mathematics, Hanover, NH 03755, USA

<sup>2</sup>Dartmouth College, Department of Economics, Hanover, NH 03755, USA

\*Corresponding author: linh.n.huynh@dartmouth.edu

<sup>e</sup>Equally-contributed co-first authors

## ABSTRACT

In recent years, Large Language Models (LLMs) have revolutionized Natural Language Processing with their ability to generate human-like texts. However, a fundamental challenge remains in understanding the underlying mechanisms driving their emergent behaviors, particularly the randomness in their outputs. This paper investigates the application of spin glass theory as a mathematical framework to quantify the uncertainty of LLMs. Moreover, we analyze how the interaction between the noise in LLMs and from social networks shape emergent collective behaviors of the system. By making connections between LLMs and spin glass models, we gain insights into the high-dimensional optimization landscapes of LLMs, the uncertainty in their outputs, and the role of noise in their learning process. We focus on LLMs' ability to replicate human-written flitizes, a form of flirtatious poems unique to Dartmouth College, used to invite peers or a potentially romantic partner to social events. Given flitizes' playful tone, personal references, and role in complex social networks, they represent a uniquely creative form of language, making them ideal for exploring how the temperature parameter in LLMs affects the creativity and verisimilitude of AI-generated content. To better understand where temperature affects model behavior, we look for temperature-based phase transitions through statistical analysis, computational methods, and simulation of our spin glass model. Our findings demonstrate that temperature not only governs randomness in LLM output, but also mediates deeper transitions in linguistic structure, perceived quality, and human-machine alignment. By connecting statistical physics with language generation, we provide a novel framework for understanding emergent behavior in LLMs and their interaction with complex social networks.

**Keywords:** Probability, Artificial Intelligence, Statistical Physics, Optimization, Social Networks, Complex Systems

## 1 Introduction

Artificial Intelligence (AI) has made significant strides in recent years, narrowing the gap between machine-produced and human-written language. These advances have sparked new debates about the role of AI in society, particularly in domains once thought to require uniquely human intelligence, such as creative writing, emotional support, and social communication. One benchmark for assessing machine intelligence—the Turing Test<sup>1</sup>, introduced by Alan Turing in 1950—posits that a machine's intelligence could be determined by its ability to exhibit behavior indistinguishable from that of a human. Other more skeptical views challenge this equivalence. For example, John Searle's Chinese Room argument<sup>2</sup> maintains that a machine's apparent grasp of language is mere symbol manipulation, devoid of true understanding—highlighting that syntactic skill alone does not equate to intelligence.

Nonetheless, recent breakthroughs in Large Language Models (LLMs), such as GPT-4<sup>3</sup> and DeepSeek<sup>4</sup>, have reignited these debates. These models now generate text with striking coherence and contextual precision, sparking both excitement and due concern about their practical application. For instance, Heinz et al. 2025<sup>5</sup> demonstrate that generative AI chat bots may offer scalable, personalized mental health interventions, an area once seen as dependent on human empathy and judgment. The success of such systems has intensified public and academic discussions over whether LLMs could augment or even supplant humans in certain jobs or creative domains, from therapy and journalism to legal analysis and romantic interaction.

Despite their impressive capabilities, LLMs continue to exhibit failure modes that challenge both their dependability and comprehensibility. These failures can range from factual inaccuracies to incoherent or biased outputs. While some stem from limitations in training data or ambiguities in the users' prompt, others emerge from more subtle, systemic phenomena rooted in the underlying architecture of the models themselves.

One particularly intriguing concept is that of phase transitions in LLM behavior. Borrowed from statistical physics, the term describes moments where small changes in model parameters—most notably, the temperature parameter that controls output randomness—can trigger abrupt, qualitative shifts in language generation<sup>6</sup>. For instance, a modest increase in temperature might cause a model’s output to move from cautious and repetitive to surprisingly erratic or imaginative. This behavioral discontinuity suggests that LLMs operate within complex, high-dimensional energy landscapes, where specific parameter thresholds can cause dramatic changes in coherence or tone.

Recent theoretical work has begun to formalize this intuition<sup>6–10</sup>. This paper will focus on one rich and underexplored genre of human communication: the Dartmouth “flitz.” A flitz—a flirtatious email often composed with rhyme or humor—is a staple of Dartmouth College’s social life, used by students to invite each other to dates, dances, or formal gatherings. Despite their playful tone, flitzes carry meaningful social weight: they express interest, recall shared experiences or inside jokes, and often showcase the sender’s unique voice and personality. Flitzes represent a distinctive type of courtship language, a category that has long fascinated linguists and anthropologists for its role in signaling affection, creativity, and social awareness. As a stylized mode of writing shaped by communal norms, they provide a rich lens for examining how language is used to express identity and emotional intent.

Recent empirical studies have complicated the assumption that human readers can reliably distinguish between AI-generated and human-written texts. For instance, Porter and Machery 2024<sup>11</sup> find that non-expert readers struggle to distinguish AI-generated poems from those written by renowned poets. Using ChatGPT-3.5 to mimic the styles of figures like Shakespeare and Whitman, they show that participants identified AI-authored poems correctly only 46.6% of the time—below chance. AI poems were not only more often mistaken for human-written but also rated higher in rhythm and beauty, as participants misapplied heuristics, mistaking simplicity for human craftsmanship and complexity for AI generation.

Other research similarly highlights the blurred boundary between human and AI communication. Kovács 2024<sup>12</sup> finds that participants struggled to accurately distinguish between human- and GPT-4-generated online reviews, even when incentivized. Both false positives (human reviews mistaken for AI) and false negatives (AI reviews mistaken for human) were common, with younger participants performing slightly better. Current AI detection systems also failed to reliably differentiate between human and AI content. Further extending this line of inquiry, Marco et al. 2025 show that even small, fine-tuned language models can match or outperform humans in short creative writing tasks. In a study comparing human-written movie synopses to those generated by BART-large, participants rated the AI-generated texts higher in readability, understandability, relevance, and attractiveness—though humans retained a slight edge in perceived creativity.

Together, these studies point to a broader phenomenon: as LLMs become more sophisticated, traditional cues that humans rely on to infer authorship—such as coherence, emotionality, and subtle stylistic markers—are increasingly unreliable. Given the growing difficulty in distinguishing human and AI-generated texts, it is critical to understand how LLMs produce language at a technical level. At their core, LLMs respond to prompts by constructing text token-by-token, using a combination of high-dimensional embeddings and attention mechanisms.

Each of tokens is mapped to a high-dimensional numerical vector called an embedding. Then, a positional encoding vector is added to each embedding to capture the order of the tokens. Corresponding to each token  $w_i$  ( $i = 1, \dots, N_W$ ) are three vectors Query  $\mathbf{q}_i$ , Key  $\mathbf{k}_i$ , and Value  $\mathbf{v}_i$  obtained by multiplying the positional embedding vector with the weight matrices  $\mathbf{W}_Q$ ,  $\mathbf{W}_K$ , and  $\mathbf{W}_V$ , which are the same for all tokens from the input prompt. Then, we compute the attention score  $(i, j)$  between token  $w_i$  and  $w_j$  by taking the inner product between  $\mathbf{q}_i$  and  $\mathbf{k}_j$ , which tells us how much attention token  $w_i$  should pay to token  $w_j$ . This attention score is scaled by the square root of the dimension of  $\mathbf{q}_i$  or  $\mathbf{k}_j$ , which should be the same. Then, the scaled attention scores are passed through the softmax function to get attention weights  $\alpha_{ij} \in [0, 1]$ . For each token  $w_i$ , we

compute (attention output) $_i := \sum_j^{N_W} \alpha_{ij} \mathbf{v}_j$ , which is then passed through a Feedforward Neural Network to allow models such as

Transformers to learn complex patterns in data. Once the tokens have gone through all transformer layers, the final embeddings, called logits, are passed through the softmax function to generate a probability distribution for selecting the next token in the sequence:  $\text{softmax}(\text{logits})_i := \frac{e^{(1/T)\text{logits}_i}}{\sum_{j=1}^{N_W} e^{(1/T)\text{logits}_j}} := \frac{e^{\beta\text{logits}_i}}{\sum_{j=1}^{N_W} e^{\beta\text{logits}_j}}$ , where  $T$  denotes the temperature parameter and  $\beta := 1/T$  is

called the inverse temperature. This softmax step determines the stochasticity of LLMs.

Intuitively, as  $T \rightarrow \infty$ ,  $P(\sigma_i)$  can be roughly viewed as  $\frac{1}{Z_N(0)}$ , which indicates approximately a uniform distribution. As  $T \rightarrow 0$ ,  $\beta \rightarrow \infty$ , if the Hamiltonian is positive, then the configuration with the highest energy dominates, making the system approximately deterministic.

An energy landscape represents the configuration space of a system, where each possible configuration corresponds to a specific energy. The local minima in the energy landscape represent stable configurations often associated with macrostates (phases) such as the ordered phase (e.g., ferromagnetic or solid) or the disordered phase (e.g., paramagnetic or liquid). As the temperature changes, the system’s thermodynamic properties (like energy, magnetization, and heat capacity) exhibit noticeable changes. At high temperatures, thermal fluctuations are large, so the system is likely to explore higher-energy configurations in the landscape. The system may explore multiple local minima but is unable to settle into a single stable state. The energy landscape appears “rough” with many small valleys (minima) separated by high-energy barriers. As a result, the system behaves in a disordered state. At low temperatures, thermal fluctuations are smaller, and the system is more likely to settle into one of the deeper local minima corresponding to a more ordered state. Here, the energy landscape appears smoother, and the system tends to have fewer configurations with low energy, leading to spontaneous ordering. At the critical temperature  $T_c$ , the system undergoes a phase transition, and the energy landscape’s structure changes dramatically. Near  $T_c$ , the landscape becomes more complex, with a narrowing of the differences between the energies of various minima. The system starts to have a larger number of competing minima that are energetically close to each other.

Spin glasses are a prototypical example of a complex disordered system in statistical mechanics. In a spin glass, the interactions between spins (magnetic moments) are randomly assigned, often with both ferromagnetic (favoring alignment) and antiferromagnetic (favoring opposite alignment) interactions. This randomness introduces disorder, as not all spins can align simultaneously in a way that minimizes energy. This competing interaction behavior is called frustration. For instance, in a ferromagnetic system, spins tend to align, but in a spin glass, some spins are forced to align oppositely due to the random nature of interactions. Spin glasses are closely related to combinatorial optimization problems, where the goal is to find the best configuration in a complex, rugged landscape. The ideas from spin glasses, particularly related to landscape complexity and frustration, are analogous to training dynamics in deep learning models. For example, neural networks can be seen as systems where training is an exploration of a rugged energy landscape with many local minima<sup>13–15</sup>.

In this paper, we ask the following questions: **(Q1)** *Can AI replicate human communication?*, **(Q2)** *At which point does AI fail to do that?*, **(Q3)** *How does the interaction between the noise in LLMs and in social networks shape emergent collective behaviors in the system?* In doing so, we focus on the specific goal of analyzing temperature-based phase transitions in people’s decision-making on distinguishing and rating human-written versus AI-generated flitzes in real data, simulated data, and the simulation of a spin glass model.

To answer the research questions, the story of our paper flows from statistical and computational analysis of data to mathematical modeling and simulation of the complex system. This paper is organized as follows. In Section 4.1, we describe our experimental design and data collection & generation. In Section 2.1, we describe our statistical analysis of the real data. In Sections 4.2 and 2.2, we describe the methods and results for our computational analysis of real and AI-generated data based on real data. In Section 4.3, we describe a mathematical model for the data and research questions. Finally, in Sections 4.4 and 2.3, we describe methods and results of simulating phase transitions in the model.

## 2 Results

### 2.1 Statistical analysis of phase transitions in data

In this section, we discuss the findings of our statistical analysis based on the 116 responses collected via Google Form described in Section 4.1. One response is excluded from the analysis, as the participant answered only a single identifying question—although a few others skipped some items, their submissions are largely complete. Our analysis examines the impact of temperature on distinguishability and perceived quality of AI-generated flitzes.

Figure 1 (A) shows the accuracy in identifying 9 pairs of human-written and AI-generated flitzes. The AI-generated flitzes were created based on virtual student profiles for each human-written flitz, and were each generated at a unique GPT-4o temperature from 0 to 2 in increments of 0.25. Looking at the AI-generated flitzes, at low temperatures,  $T \in [0, 1.00)$ , the probability distribution over the next token is sharply peaked, favoring high-likelihood continuations. As a result, AI-generated flitzes are more conservative and resulting accuracies are near the 50% level. At  $T = 1.25$ , a local minimum occurs, with only 41% of responses correctly identifying the flitz as AI-generated. At higher temperatures,  $T \in [1.50, 2.00]$ , the probability distribution

flattens, allowing lower-probability tokens a better chance of being selected. At this point, accuracy rises significantly, peaking at a local maximum of 91% at  $T = 1.75$ . This is likely due to the fact that the language generated becomes so erratic that respondents could easily identify it as not human-written.

Figure 1 (B) shows the absolute difference from 50%, plot at each temperature for the same 9 AI-generated flitzes. This figure assess how far accuracy deviates from what would be expected under random binary choice. We see that flitzes with temperature at  $T = 0.25$  and  $T = 0.5$  show minimal deviation, suggesting that participants were effectively guessing, consistent with the law of large numbers for flipping an unbiased coin. As the temperature increases, the deviation grows, peaking at  $T = 1.75$ , where responses are furthest from random chance. These results show that participant behavior transitions from approximating an unbiased coin flip to exhibiting clear signal detection. If we assume that there is no bias, then distinguishing AI-generated versus human-written flitzes is like flipping a coin. By Law of Large Numbers, as the number of flips increases, the proportion of heads (or tails) will tend to get closer and closer to 50%, making the theoretical probability of accuracy  $\frac{1}{2}$ . To reiterate, we observe that the absolute difference is significantly smaller for low temperatures i.e.  $T \in [0, 1.00]$  than for high temperatures, i.e.  $T \in [1.00, 2.00]$ . This is consistent with the design of LLMs, where the higher the temperature, the more creative, or random, LLMs' responses are.

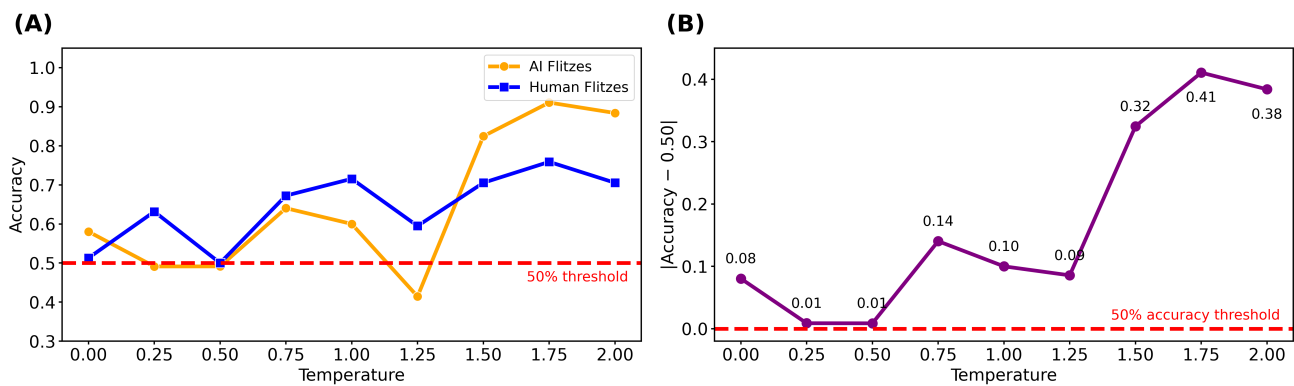
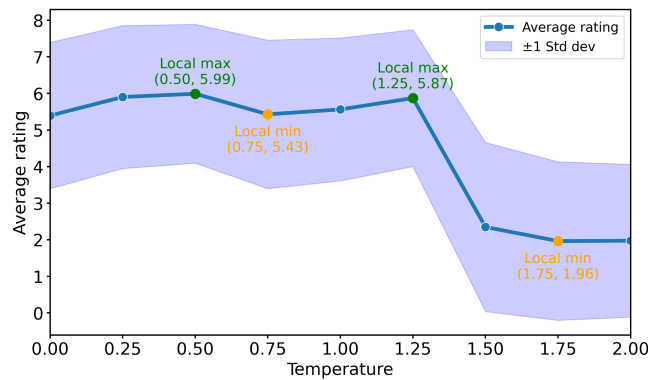


**Figure 1. Statistical analysis of the temperature's effect on distinguishing accuracy in real data.** (A): Accuracy in identifying AI-generated flitzes, each created at a unique temperature from 0 to 2 in increments of 0.25. At low temperatures ( $T \in [0, 1.00]$ ), AI-generated flitzes mimic human tone, leading to near-random accuracy. Accuracy generally rises with temperature, peaking at  $T = 0.75$ . Accuracy drops again below random chance at  $T = 1.25$ , before rising sharply to a local maximum at  $T = 1.25$ , when AI-generated outputs become noticeably erratic. (B): Absolute difference from 50% accuracy by temperature. Minimal deviation at  $T = 0.25$  and  $0.5$  suggests guessing behavior, consistent with the law of large numbers for flipping an unbiased coin. As temperature increases, clearer signals of AI authorship emerge, with deviation peaking at  $T = 1.75$ , where responses are furthest from random chance.

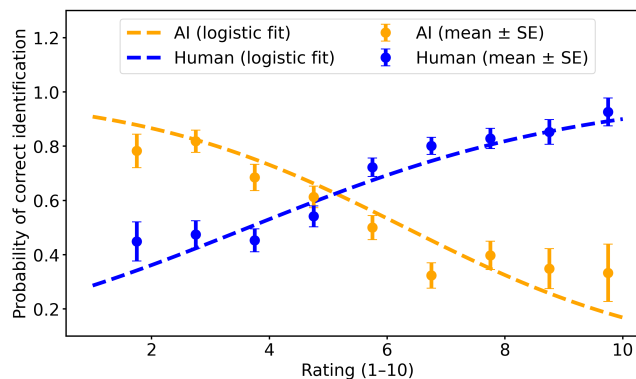
Figure 2 shows perceived quality ratings (scale of 1 – 10, with 1 being "very poor" and 10 being "excellent") for the same set of AI-generated flitzes, with shaded regions representing  $\pm 1$  standard deviation. A local maximum is observed at  $T = 0.5$ , suggesting that outputs at this temperature were perceived as the most coherent and engaging. Ratings dip to a local minimum at  $T = 0.75$ , before rising again to a secondary peak at  $T = 1.25$ . Interestingly, this is the same temperature at which mean cosine similarity scores for our simulated data dramatically shift downwards, as discussed in 2.2, suggesting a structural transformation in AI outputs aligned with human perceptual thresholds. Beyond this, ratings drop dramatically, indicating that the outputs became erratic, stylistically unappealing, or even incoherent. This indicates that there exists a "sweet spot" of originality and coherence at a moderate temperature. This is somewhat surprising, given that ChatGPT-4o is believed to operate at a different default temperature (likely  $T \in [0.70, 1.00]$ ).

Figure 3 illustrates the relationship between the participants' perceived quality of a flitz on a scale from 1-10 and whether they correctly identified its author as AI or human. A logistic regression curve is fitted separately for the mean data for AI-generated and human-written flitzes. For AI flitzes (plotted in orange), higher ratings were associated with lower probabilities of correct identification, meaning AI-generated flitzes become harder to identify and more likely to be mistaken as human-written. Conversely, human-written flitzes (plotted in blue), show the opposite trend: higher rated flitzes were more likely to be correctly

identified as written by a human. As an example, the orange curve reveals that when a flitz is human-written and rated a 1, only about 30% of respondents correctly identify its origin. On the other hand, the blue curve shows that when a flitz is AI-generated and also rated as 1, over 90% of respondents classify it as AI. Overall, this divergence allows us to conclude that "better" AI-generated flitzes effectively mimic the stylistic cues of genuine human language.



**Figure 2. Statistical analysis of the temperature’s effect on rating of AI-generated flitzes in real data.** Perceived quality ratings (scale of 1 – 10) for the same set of AI-generated flitzes, with shaded bands showing  $\pm 1$  standard deviation. Ratings peak at  $T = 0.5$ , dip at  $T = 0.75$ , and rise to a secondary peak at  $T = 1.25$ , reflecting an interesting relationship – higher rated AI-generated flitzes are harder to identify as being AI-generated. Beyond  $T = 1.25$ , average ratings fall sharply. This suggests a "sweet spot" for coherence and originality at moderate temperatures, surprisingly not at ChatGPT-4o’s default (likely  $T \in [0.70, 1.00]$ ).



**Figure 3. Correlation between perceived quality and correction identification of AI vs. human flitzes.** This figure shows how the perceived quality of flitzes relate to correct identification. A logistic regression curve is fitted separately for the mean data for AI-generated and human-written flitzes. For AI-generated flitzes (orange), higher ratings lowered the chance of correct classification—better ones were often mistaken for human. For human flitzes (blue), higher ratings were correlated with correct identification. This suggests that "better" AI-generated flitzes effectively imitate human stylistic cues.

## 2.2 Computational analysis of phase transitions in data

In this section, we analyze the structural divergence between AI-generated and human-written flitzes, using both cosine similarity and Wasserstein distance. Both metrics provide evidence for a temperature-induced phase transition in the language structure of AI-written flitzes between  $T = 1.25$  and  $T = 1.38$ .

Figure 4 (A) shows the kernel density estimation (KDE) distributions of cosine similarity scores between human-written and AI-generated flitzes at different temperature values. KDE distribution is a smoothed version of a histogram which estimates the probability density function for a variable. We collected 33 human-written flitzes from students at Dartmouth, and then used ChatGPT to generate 33 corresponding virtual student profiles – one for each human-written flitz. Then, we generated 10 flitzes with ChatGPT-4o for each virtual student profile at each of 17 temperature values (from 0 to 2 in increments of 0.125), giving us a total of  $33 \cdot 10 \cdot 17 = 5610$  flitzes. For each pair of human-written and AI-generated flitzes, we computed

the cosine similarity using TF-IDF vectorization of the flitz content. At lower temperatures ( $T \in [0, 1.00]$ ), the AI-generated flitzes remain closer in content to their human-written pairs. Around  $T = 1.25$ , the cosine similarity scores shift downward, reflecting increased creative randomness in the AI’s language generation. Figure 4 (B) shows cosine similarity scores, averaged across all samples, at each temperature value, with an error bar representing  $\pm 1$  standard deviation. Here, we assume that each sample is independent and identically distributed (iid). Again, for  $T \in [0, 1.00]$ , the mean similarity stays roughly constant, which suggests that the outputs are stylistically similar to the human-written flitzes. However, there is a sharp decline between  $T = 1.25$  and  $T = 1.38$ . This suggests a phase transition in the language structure of the AI-generated flitzes. After  $T = 1.50$ , the average similarity score settles near zero, which indicates that the AI-generated flitzes at high temperature values are fundamentally dissimilar to their human-written pairs.

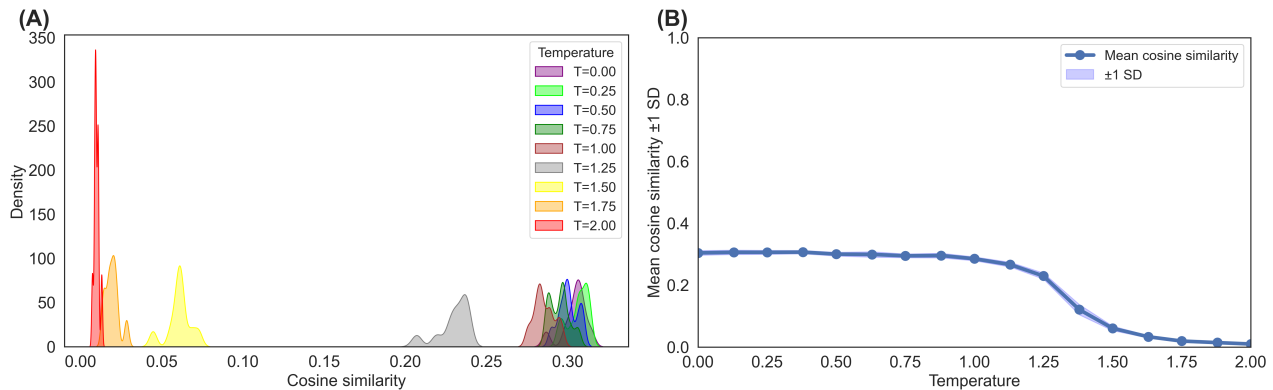


**Figure 4. Probability distribution of cosine similarity for different temperatures in simulated data with combined flitzes.** (A): For each pair of human-written and AI-generated flitzes, we compute the cosine similarity using TF-IDF vectorization. This plot shows the full distribution of those cosine similarity scores, for 9 selected temperature values, via kernel density estimation (KDE). At lower temperatures, the AI-generated flitzes remain closer in content to their human-written counterparts, demonstrated by the cluster appearing on the right end of the x-axis. As temperature increases, particularly around  $T = 1.25$  (the probability distribution in grey), the cosine similarity scores shift downward, reflecting creative randomness in the AI’s language generation. Another cluster appears near cosine similarity scores of 0 for high temperature values ( $T \in [1.50, 2.00]$ ), demonstrating significant dissimilarity with their human-written counterparts. (B): This figure shows the average cosine similarity between human-written and AI-generated flitzes at each temperature value, with an error bar representing  $\pm 1$  standard deviation. We assume that the data for each sample is independent and identically distributed (iid). For temperatures  $T \in [0, 1.00]$ , the average similarity stays roughly constant, suggesting that the outputs are stylistically similar. However, the sharp decline between  $T = 1.25$  and  $T = 1.38$  suggests a phase transition in the language’s structure. After  $T = 1.50$ , the average similarity score plateaus near zero, indicating that the AI-generated flitzes are fundamentally dissimilar to the human-written ones.

Figure 5 further quantifies the shift in similarity using Wasserstein distance. In Figure 5 (A), we plot the Wasserstein distance between probability distributions for cosine similarity scores between consecutive temperatures (i.e. between  $T_k$  and  $T_{k+1}$ ). The distance between lower temperature values hovers around zero, up to around  $T = 1.00$ . There is a sharp increase in the distance between  $T = 1.25$  and  $T = 1.38$ , indicating a sudden shift, or phase transition, in the structure of the text generation. The distance then drops again, reflecting that probability distributions at high temperatures are consistently dissimilar from those at low temperatures, but that the probability distributions at high temperatures are relatively stable among themselves. Figure 5 (B) provides another representation of this phase transition. We computed the Wasserstein distance between the probability distribution at each temperature compared to the baseline distribution at  $T = 0$ . The curve remains roughly flat until  $T = 1.00$ , indicating similarity in the structure of AI-generated flitzes at low temperatures. A pronounced jump occurs at  $T = 1.38$ , reflecting a sudden shift in ChatGPT’s output. The curve plateaus around  $T = 1.63$ , which indicates limited further shifts in the language structure of the output. Together, these results demonstrate that a clear phase transition occurs in the structure of the AI-generated flitzes between  $T = 1.25$  and  $T = 1.38$ . Beyond this point, the similarity of AI-generated flitzes and human-written flitzes dramatically decreases, and further structural changes at higher temperature values become minimal.

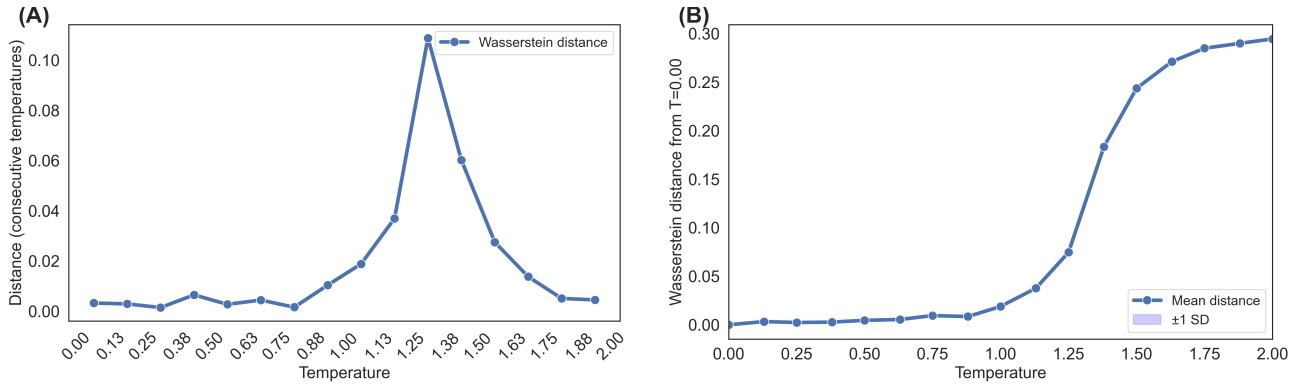


**Figure 5. Distances between probability distributions of cosine similarity for different temperatures in simulated data with combined flitzes.** (A): This plot shows the Wasserstein distance between probability distributions for cosine similarity scores between consecutive temperatures (i.e. between  $T_k$  and  $T_{k+1}$ ). The distance measures how much probability distributions shift as the temperature increases. There is a sharp spike in the distance between  $T = 1.25$  and  $T = 1.38$ , suggesting a sudden shift in the structure of the underlying text generation. Here, we assume that the probability distributions at each temperature value are independent and identically distributed (iid). (B): This figure plots the Wasserstein distance between the probability distribution for cosine similarity scores at each temperature and the baseline distribution at temperature 0. The curve remains relatively flat at lower temperature scores, with a modest increase occurring between temperature values  $T = 1.00$  and  $T = 1.25$ . The most pronounced jump occurs at  $T = 1.38$ , before the curve plateaus around  $T = 1.63$ .

### 2.3 Simulated phase transitions in spin glass model

In this section, we analyze how stochasticity in the social network influences phase transitions in LLMs.

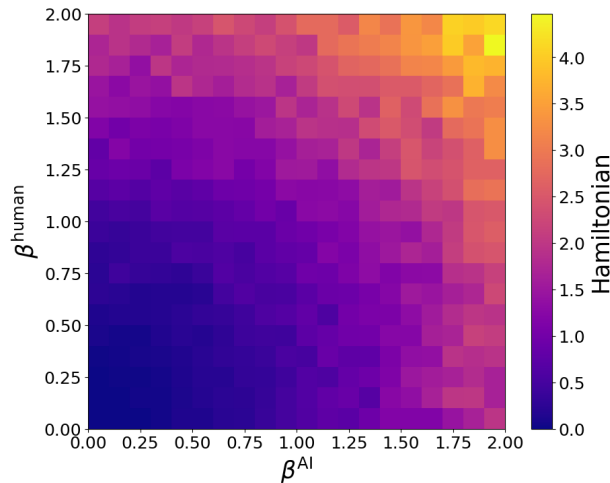


**Figure 6. Phase diagram showing the average system energy (Hamiltonian) as a function of the inverse temperatures  $\beta^{\text{AI}}$  and  $\beta^{\text{human}}$ .** Each point represents the mean energy computed over multiple Metropolis-Hastings updates following a burn-in period, where individuals interact with both human-generated and AI-generated features. The color intensity indicates the energy level, revealing distinct regimes of system behavior depending on the influence of human versus AI factors. The figure shows a quadratic curve for a phase transition.

Figure 6 shows a phase diagram that visualizes the average energy of a system consisting of multiple species (people, human-written flitzes, and AI-written flitzes) as a function of two key parameters: the inverse temperature parameters  $\beta^{\text{human}}$  and  $\beta^{\text{AI}}$ . The axes represent the values of  $\beta^{\text{human}}$  on the x-axis and  $\beta^{\text{AI}}$  on the y-axis, both ranging from 0 to 2.00. The color intensity within the diagram corresponds to the average energy of the system, with darker shades indicating lower energy and lighter shades representing higher energy configurations. Consistent with the results of our statistical analysis, at higher  $\beta$  (lower temperatures), the human-written and AI-written flitzes are viewed more favorably, demonstrated by a higher energy configuration. The heatmap is generated by simulating the system using a Metropolis-Hastings update for each combination of

$\beta^{\text{human}}$  and  $\beta^{\text{AI}}$ , and calculating the average energy over a set number of steps after a burn-in period. The resulting matrix is then displayed as an image, with a colorbar indicating the corresponding values of the average energy.

### 3 Conclusion and Discussion

Our study investigates how varying the temperature parameter in Large Language Models (LLMs) induces phase transitions in AI-generated language, using Dartmouth "flitzes" as a test case. Our main results are as follows: **(R1)** Statistical analysis on real data reveals that at low temperatures, accuracy in distinguishing between AI-generated and human-written text hovers around 50%, consistent with random guessing per the Law of Large Numbers. At higher temperatures, this law does not hold. In contrast, existing spin glass theory results show that Law of Large Numbers hold for the partition function  $Z_N(\beta)$  at high temperatures but not low temperatures<sup>16,17</sup>. **(R2)** Both statistical analysis on real data (capturing human bias and perception) as well as cosine similarity and Wasserstein distance analyses show a sharp structural shift in AI-generated flitzes between  $T = 1.25$  and  $T = 1.38$ . At lower temperatures, AI output closely mimics human-written language, but beyond this threshold, the generated text becomes increasingly dissimilar.

Several limitations in our methodology merit discussion. First, our study's focus on Dartmouth "flitzes," a socially-specific form of language, may limit the generalizability of our findings. The respondents to our distinguishing human-written and AI-generated flitzes survey were not drawn exclusively from Dartmouth, but flitzes are culturally idiosyncratic, and they may not generalize to broader forms of AI-human interaction or social language. Second, temperature was the only generation parameter that we varied in our study. This allowed us to isolate the effects of temperature on the model's output, but it does not address how other parameters, such as top-p or min-p sampling<sup>18</sup>, could confound the temperature-induced phase transitions we discovered. Third, our AI-written flitz generation methodology may constrain the range of generated styles given its recursive approach. We obtained our virtual student profiles by prompting ChatGPT to summarize the traits of each real flitz author. We attempted to present a diverse array of flitzing styles through our sample of 33 flitzes, but this approach may have limited the range of possible ChatGPT outputs for AI-written flitzes, especially at lower temperatures. Finally, all AI-written flitzes in our study were produced using ChatGPT-4o. This version is one of the most advanced publicly available LLMs, but relying on a single model limits our ability to generalize our findings to all LLMs.

These limitations suggest several directions for future research. First, future studies could replicate our analysis in other, more generalizable, forms of language, such as poetry or workplace emails. This would aid in assessing the generalizability of our findings beyond the socially-specific language form of Dartmouth flitzes. Second, future work could explore other generation parameters to determine whether their interactions with temperature shape temperature-induced phase transitions. Third, to address the potential stylistic constraints introduced by our AI-written flitz generation methodology, future studies could consider building virtual profiles manually or using a more diverse set of prompts to generate virtual profiles. Finally, replicating our analysis across a range of LLM architectures, such as Claude, Mistral, or future OpenAI models, would clarify whether the temperature-induced phase transitions we observe are specific to ChatGPT-4o or are a feature of large-scale LLMs.

Beyond our specific application to flitzes, our work has broader implications for the study of emergent behavior in AI-human systems. By framing AI-human interaction as a coupled spin glass system, we identify phase transitions that mark critical shifts in coherence, authenticity, and mutual intelligibility<sup>19,20</sup>. This paradigm not only connects statistical physics with natural language processing and social network theory, but also opens the pathway to study the evolution of language and social norms under artificial intelligence<sup>21,22</sup>. As AI influences human language, which then influences AI training, our language system is actively adapting with artificial agents<sup>23,24</sup>. The same tools that describe magnetism and disorder in physical systems may now illuminate how creativity, empathy, and trust unfold in machine-mediated relationships<sup>13,15</sup>. As AI systems gain prominence in all forms of communication, our findings raise essential questions: What does it mean for language to be "human"? Should generative models be tasked with delivering messages of love or support that humans perceive as more thoughtful than real human responses? In charting these phase transitions, we can mitigate dangerous or unpredictable behaviors in LLMs, whether in social media ecosystems, collaborative workspaces, or education curricula. Through our research, we take a first step toward building models that are not just intelligent, but interpretable, ethical, and aligned with the values of the societies they inhabit.

## 4 Methods

### 4.1 Experimental design and data generation

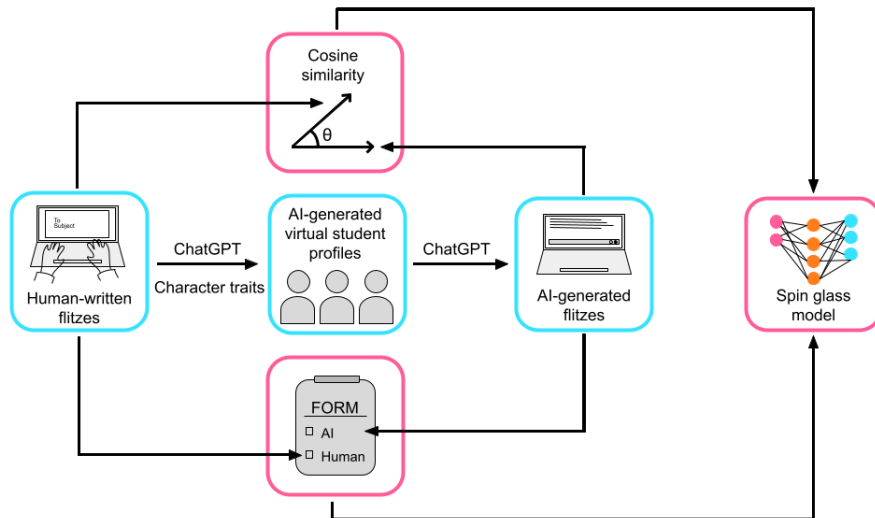


**Figure 7. Schematic diagram of experimental design and data generation.** Blue boxes indicate dataset components, and pink boxes indicate methods. We collected 33 human-written flitzes from members of the Dartmouth community, which we used to generate 33 "virtual student profiles" using ChatGPT. These were used to generate flitzes for each profile across 17 different temperature values. Cosine similarity was then computed between human-written and AI-generated flitzes. A Google Form collected human/AI classifications and perceived quality ratings. Finally, all outputs were analyzed through a spin glass model to characterize phase transition behavior in the generation of text.

In this section, we describe the experimental design and data collection depicted in Figure 7. We designed a two-part experiment combining synthetic data generation with human evaluation. We begin by collecting 33 human-written flitzes from Dartmouth students. Each flitz was then input into ChatGPT to create 33 virtual student profiles generated at the default ChatGPT temperature, each reflecting distinctive stylistic traits such as tone, humor, flirtation style, and language quirks. For each profile, ChatGPT produced 10 independent samples of AI-generated flitzes at 17 temperature values in increments of 0.125: {0.00, 0.13, 0.25, 0.38, ..., 1.75, 1.88, 2.00}. For each sample, we cycled through all 33 virtual student profiles and prompted the model to generate one flitz per profile, using the following base prompt format:

"Read these articles so you know what a flitz is: <https://www.thedartmouth.com/article/2022/11/the-art-of-flitzing-amell-angst> and <https://www.nhpr.org/nh-news/2023-02-14/a-flirtatious-email-that-rhymes-dartmouth-undergrads-send-them-all-the-time>. Write me a flitz, acting as a student with the following profile: [insert virtual student traits]."

This resulted in a total of 5,610 AI-generated flitzes (33 flitzes  $\times$  10 samples  $\times$  17 temperature levels). All generations were capped at a maximum length of 500 tokens. Other model parameters (e.g., top-p, frequency penalty) were held constant to ensure that temperature was the only varying factor. For downstream human evaluation, a subset of these flitzes was selected, excluding examples that contained overtly non-human content or self-referential language indicative of AI generation.

We then compute cosine similarity scores between each human-written flitz and its AI-generated counterparts using TF-IDF vectorization, allowing us to quantify textual and stylistic divergence across temperatures. We evaluated human perception of flitzes using a blind survey distributed via Google Forms. Participants were recruited both from Dartmouth College and externally, resulting in a diverse respondent pool. In total, 116 participants completed the survey. Each participant viewed 9 human-written and 9 AI-generated flitzes and completed two tasks: (1) rating each flitz on a scale from 1 (worst) to 10 (best)

based on perceived quality, and (2) guessing whether the flitz was authored by a human or by AI. Flitzes were curated to ensure a balance of tone, content, and demographic relevance. Finally, both the cosine similarity and the distinguishing/rating results were analyzed through the lens of a spin glass model, capturing how small changes in temperature give rise to large, non-linear shifts in text structure—analogueous to phase transitions in complex systems.

This experimental design allowed robust quantitative and qualitative analyses of how temperature affects the linguistic structure and human reception of LLM output. These data form the basis for the statistical inference, phase-transition modeling, and spin glass simulations presented in subsequent sections.

## 4.2 Cosine similarity, TF-IDF, and Wasserstein distance

In this section, we describe the methods used for computational analysis of phase transitions in our simulated data. Cosine similarity between two vectors  $u$  and  $v$  is defined as cosine of the angle between them:

$$\text{cosine similarity}(u, v) = \frac{u \cdot v}{\|u\| \|v\|} \quad (1)$$

where  $u \cdot v$  is the inner product of the two vectors  $u$  and  $v$ ,  $\|u\|$  and  $\|v\|$  are the magnitudes (usually Euclidean norms) of the vectors  $u$  and  $v$ , respectively. The result of the cosine similarity calculation ranges from -1 to 1 in general: 1 means that the vectors are identical (i.e., the angle between them is 0 degrees), 0 means that the vectors are orthogonal (i.e., no similarity), -1 indicates that the vectors are diametrically opposite (i.e., the angle between them is 180 degrees). However, in our application, the values range from 0 to 1 because we compute cosine similarity using TF-IDF vector representations of the flitzes; specifically, we use `TfidfVectorizer()` from the `scikit-learn` Python package. Since TF-IDF vectors are non-negative by construction, the dot product of the two vectors will always be non-negative, so the cosine similarity value is bounded in  $[0, 1]$ , with 1 indicating that the vectors are identical, and 0 indicating that they are completely orthogonal (i.e. no overlap in vocabulary usage).

TF-IDF (term frequency-inverse document frequency) is a natural language processing technique for analyzing the importance of words in a document corpus. Term frequency (TF) measures the frequency of a word in a given document, and inverse document frequency (IDF) measures the rarity of that word across a corpus of documents. Mathematically, the TF-IDF score is given by:

$$\text{TF-IDF}(t, d) = (1 + \log(\text{tf}_{t,d})) \cdot \log\left(\frac{1 + N}{1 + \text{df}_t}\right) + 1 \quad (2)$$

where  $\text{tf}_{t,d}$  is the raw count of term  $t$  in document  $d$ ,  $\text{df}_t$  is the number of documents containing term  $t$ , and  $N$  is the total number of documents in the corpus.<sup>25</sup> We use TF-IDF vectors to compute cosine similarity between human-written and AI-generated flitz pairs, as discussed in 2.2. To further visualize the temperature-induced phase transition in our AI-generated flitzes, we calculate the Wasserstein distance between cosine similarity probability distributions.

The Wasserstein distance<sup>26,27</sup> is a measure of the difference between two probability distributions. Mathematically, for two distributions  $\mu$  and  $\nu$  over a metric space  $\mathcal{X}$ , the  $p$ -th Wasserstein distance is defined as:

$$W_p(\mu, \nu) = \left( \inf_{\gamma \in \Gamma(\mu, \nu)} \int_{\mathcal{X} \times \mathcal{X}} d(x, y)^p d\gamma(x, y) \right)^{1/p} \quad (3)$$

Here,  $\Gamma(\mu, \nu)$  denotes the set of all couplings between  $\mu$  and  $\nu$ ,  $d(x, y)$  is the distance metric between points  $x$  and  $y$ , and the infimum is taken over all possible couplings. In the case of  $p = 1$ , this gives the Wasserstein-1 distance, which measures the minimal amount of "work" required to move probability mass from one distribution to another. This distance captures both the mass and the geometry of the distributions, making it more robust than other divergence measures like Kullback-Leibler divergence.

## 4.3 Mathematical spin glass model

In this section, we build a spin glass model for our AI-human interaction networks. Spin glasses can be viewed as large random networks where each node interacts with others through random edges. These disordered interactions create a complex energy landscape with many competing states, leading to frustration, metastability, and rich collective behavior. We model our complex system of AI-human random interaction networks with two coupled multi-species bipartite Sherrington–Kirkpatrick (SK) model, which are a generalization of the classical SK spin glass model<sup>19</sup> that incorporates both species heterogeneity and a bipartite

interaction structure. In a bipartite structure, individuals are divided into distinct groups (species), and interactions occur only between, not within, these groups, forming a bipartite graph. Each species can have different sizes and interaction variances, allowing the model to capture more complex and realistic systems, such as in biological<sup>21,28</sup> and social systems<sup>22</sup>. Mathematical analysis of this type of model are actively researched by Erik Bates & Youngtak Sohn<sup>20,29</sup> and Elizabeth Collins-Woodfin & Han Gia Le<sup>30,31</sup>. In general, a multi-species bipartite SK spin glass model is described as follows. Given two species that have  $n$  and  $m$  individuals, denote two corresponding spin variables/network configurations as  $\sigma$  and  $\tau$  respectively:

$$\sigma = (\sigma_1, \sigma_2, \dots, \sigma_n) \in S_{n-1} \quad \tau = (\tau_1, \tau_2, \dots, \tau_m) \in S_{m-1}, \quad (4)$$

where  $S_{n-1} = \{u \in \mathbb{R}^n : \|u\|^2 = n\}$ . The Hamiltonian for the model is:

$$\mathcal{H}(\sigma, \tau) = \frac{1}{\sqrt{n+m}} \sum_{i=1}^n \sum_{j=1}^m J_{ij} \sigma_i \tau_j \quad \text{with} \quad J_{ij} \sim \text{Normal}(0, 1). \quad (5)$$

The Gibbs measure for this model at inverse temperature  $\beta > 0$  is:

$$p(\sigma, \tau) = \frac{1}{Z_{n,m}} e^{\beta \mathcal{H}(\sigma, \tau)} \quad \text{with} \quad Z_{n,m} = \int_{S_{m-1}} \int_{S_{n-1}} e^{\beta \mathcal{H}(\sigma, \tau)} d\omega_n(\sigma) d\omega_m(\tau), \quad (6)$$

where  $d\omega_n$  is the uniform probability measure on  $S_{n-1}$ .

Our complex system consists of people, human-written flitzes, and AI-generated flitzes. We consider two multi-species bipartite SK spin glass models. The first one is between people and human-written flitzes, and the second one is between the same people and AI-generated flitzes. Hence, these two multi-species bipartite SK spin glass models are coupled by the same set of people. Denote:

$$X := (X_1, X_2, \dots, X_{n_{\text{people}}}) \in S_{n_{\text{people}}-1} \quad \text{represents personalities of one person,} \quad (7)$$

$$F^{\text{human}} := (F_1^{\text{human}}, F_2^{\text{human}}, \dots, F_{n_{f_h}}^{\text{human}}) \in S_{n_{f_h}-1} \quad \text{represents dual personality values of a human-written flitz,} \quad (8)$$

$$F^{\text{AI}} := (F_1^{\text{AI}}, F_2^{\text{AI}}, \dots, F_{n_{f_{\text{AI}}}}^{\text{AI}}) \in S_{n_{f_{\text{AI}}}-1} \quad \text{represents dual personality values of an AI-generated flitz.} \quad (9)$$

The multi-species bipartite spherical SK model for the person and a human-written flitz is defined with the following Hamiltonian:

$$\mathcal{H}(X, F^{\text{human}}) = \frac{1}{\sqrt{n_{\text{people}} + n_{f_h}}} \sum_{i=1}^{n_{\text{people}}} \sum_{j=1}^{n_{f_h}} J_{ij}^{\text{human}} X_i F_j^{\text{human}} \quad \text{with} \quad J_{ij}^{\text{human}} \sim \text{Normal}(0, 1) \quad (10)$$

and the corresponding Gibbs measure with inverse temperature  $\beta^{\text{human}} > 0$  is:

$$p(X, F^{\text{human}}) = \frac{1}{Z_{n_{\text{people}}, n_{f_h}}} e^{\beta^{\text{human}} \mathcal{H}(X, F^{\text{human}})} \quad \text{with} \quad Z_{n_{\text{people}}, n_{f_h}} = \int_{S_{n_{f_h}-1}} \int_{S_{n_{\text{people}}-1}} e^{\beta^{\text{human}} \mathcal{H}(X, F^{\text{human}})} d\omega_{n_{\text{people}}}(X) d\omega_{n_{f_h}}(Y). \quad (11)$$

The multi-species bipartite SK model for the person and an AI-generated flitz is defined with the following Hamiltonian:

$$\mathcal{H}(X, F^{\text{AI}}) = \frac{1}{\sqrt{n_{\text{people}} + n_{f_{\text{AI}}}}} \sum_{i=1}^{n_{\text{people}}} \sum_{j=1}^{n_{f_{\text{AI}}}} J_{ij}^{\text{AI}} X_i F_j^{\text{AI}} \quad \text{with} \quad J_{ij}^{\text{AI}} \sim \text{Normal}(0, 1). \quad (12)$$

and the corresponding Gibbs measure with inverse temperature  $\beta^{\text{AI}} > 0$  is:

$$p(X, F^{\text{AI}}) = \frac{1}{Z_{n_{\text{people}}, n_{f_{\text{AI}}}}} e^{\beta^{\text{AI}} \mathcal{H}(X, F^{\text{AI}})} \quad \text{with} \quad Z_{n_{\text{people}}, n_{f_{\text{AI}}}} = \int_{S_{n_{f_{\text{AI}}}-1}} \int_{S_{n_{\text{people}}-1}} e^{\beta^{\text{AI}} \mathcal{H}(X, F^{\text{AI}})} d\omega_{n_{\text{people}}}(X) d\omega_{n_{f_{\text{AI}}}}(F^{\text{AI}}). \quad (13)$$

The extent to which these personalty values and dual personality values is encoded in the matrix  $J_{ij}$ . Hamiltonian expresses the human response to the flitz, similar to the data in Figure 1.

#### 4.4 Numerical simulation of phase transitions

We simulate the coupled bipartite spin glass system using a Metropolis–Hastings algorithm to sample from the joint Gibbs distribution over people, human-written flitzes, and AI-generated flitzes. Each entity is represented by a unit vector on a high-dimensional sphere, and proposed updates involve Gaussian perturbations followed by projection onto the sphere to preserve normalization. At each iteration, the acceptance of a new configuration is determined by the Metropolis criterion, based on the change in total Hamiltonian energy weighted by inverse temperature parameters  $\beta^{\text{human}}$  and  $\beta^{\text{AI}}$ . For each pair  $(\beta^{\text{human}}, \beta^{\text{AI}})$  on a regular grid, the system undergoes a burn-in phase to reach equilibrium, followed by a sampling phase during which statistical observables are computed. These include the average energy, the overlaps between people and each type of flitz, and the overlap between human- and AI-generated flitzes. Overlaps are defined as mean inner products between vector sets, quantifying alignment in latent perceptual space. The resulting measurements are assembled into phase diagrams and cross-sectional plots to examine how collective alignment and preference structure vary with thermal noise, as controlled by  $\beta$ . A new configuration  $X'_i$  is proposed by perturbing  $X_i$  with Gaussian noise and projecting it onto the sphere. The acceptance probability for the update is:

$$P_{\text{accept}} = \min \left( 1, \exp \left( -\beta^{\text{human}} \left( \mathcal{H}(X', F^{\text{human}}) - \mathcal{H}(X, F^{\text{human}}) \right) \right. \right. \quad (14)$$

$$\left. \left. -\beta^{\text{AI}} \left( \mathcal{H}(X', F^{\text{AI}}) - \mathcal{H}(X, F^{\text{AI}}) \right) \right) \right), \quad (15)$$

where  $\beta^{\text{human}}$  and  $\beta^{\text{AI}}$  are the inverse temperatures. The average energy is computed by summing the Hamiltonians for the human-written flitzes and AI-generated flitzes, then averaging over a specified number of steps. The total energy  $\mathcal{H}_{\text{total}}$  at each step is given by:

$$\mathcal{H}_{\text{total}} = \beta^{\text{human}} \cdot \mathcal{H}(X, F^{\text{human}}) + \beta^{\text{AI}} \cdot \mathcal{H}(X, F^{\text{AI}}), \quad (16)$$

where  $\beta^{\text{human}}$  and  $\beta^{\text{AI}}$  are the inverse temperatures,  $\mathcal{H}(X, F^{\text{human}})$  is the Hamiltonian for the interaction between people and human-written flitzes,  $\mathcal{H}(X, F^{\text{AI}})$  is the Hamiltonian for the interaction between people and AI-generated flitzes. Each Hamiltonian is calculated as:

$$\mathcal{H}(X, F) = \frac{1}{\sqrt{n_{\text{people}} + n_f}} \sum_{i=1}^{n_{\text{people}}} \sum_{j=1}^{n_f} J_{ij} X_i \cdot F_j, \quad (17)$$

The average energy is then computed by averaging over the total energy across multiple steps:

$$\langle \mathcal{H}_{\text{total}} \rangle = \frac{1}{n_{\text{steps}}} \sum_{t=1}^{n_{\text{steps}}} \mathcal{H}_{\text{total}}(t), \quad (18)$$

where  $\mathcal{H}_{\text{total}}(t)$  is the total energy at the  $t$ -th step, and  $n_{\text{steps}}$  is the number of steps used for sampling. We compute this quantity for a range of inverse temperatures  $\beta^{\text{human}}$  and  $\beta^{\text{AI}}$ , generating heat maps to study phase transitions in terms of  $(\beta^{\text{AI}}, \beta^{\text{human}})$ . We estimate the free energy of the coupled bipartite spherical SK model using Monte Carlo simulation. The procedure consists of the following steps:

1. Sample disorder: Draw the random interaction matrices

$$J_{ij}^{\text{human}} \sim \mathcal{N}(0, 1), \quad J_{ij}^{\text{AI}} \sim \mathcal{N}(0, 1), \quad (19)$$

for  $i = 1, \dots, n_{\text{people}}$ ,  $j = 1, \dots, n_{f_h}$  or  $n_{f_{\text{AI}}}$  respectively.

2. Generate spherical spin configurations: Sample spin vectors

$$X \in \mathcal{S}_{n_{\text{people}}-1}, \quad F^{\text{human}} \in \mathcal{S}_{n_{f_h}-1}, \quad F^{\text{AI}} \in \mathcal{S}_{n_{f_{\text{AI}}}-1} \quad (20)$$

uniformly from their respective unit spheres.

3. Evaluate the joint Hamiltonian:

$$\mathcal{H}_{\text{joint}}(X, F^{\text{human}}, F^{\text{AI}}) = \beta^{\text{human}} \mathcal{H}(X, F^{\text{human}}) + \beta^{\text{AI}} \mathcal{H}(X, F^{\text{AI}}), \quad (21)$$

where each component is given by

$$\mathcal{H}(X, F^{\text{human}}) = \frac{1}{\sqrt{n_{\text{people}} + n_{f_h}}} \sum_{i,j} J_{ij}^{\text{human}} X_i F_j^{\text{human}}, \quad (22)$$

$$\mathcal{H}(X, F^{\text{AI}}) = \frac{1}{\sqrt{n_{\text{people}} + n_{f_{\text{AI}}}}} \sum_{i,j} J_{ij}^{\text{AI}} X_i F_j^{\text{AI}}. \quad (23)$$

## References

1. French, R. M. The turing test: the first 50 years. *Trends cognitive sciences* **4**, 115–122 (2000).
2. Searle, J. The chinese room (1999).
3. Achiam, J. *et al.* Gpt-4 technical report. *arXiv preprint arXiv:2303.08774* (2023).
4. Liu, A. *et al.* Deepseek-v3 technical report. *arXiv preprint arXiv:2412.19437* (2024).
5. Heinz, M. V. *et al.* Randomized trial of a generative ai chatbot for mental health treatment. *NEJM AI* **2**, AIoa2400802 (2025).
6. Nakaishi, K., Nishikawa, Y. & Hukushima, K. Critical phase transition in large language models. *arXiv preprint arXiv:2406.05335* (2024).
7. Arnold, J., Holtorf, F., Schäfer, F. & Lörch, N. Phase transitions in the output distribution of large language models. *arXiv preprint arXiv:2405.17088* (2024).
8. Mikhaylovskiy, N. States of llm-generated texts and phase transitions between them. *arXiv preprint arXiv:2503.06330* (2025).
9. Evstafev, E. The paradox of stochasticity: Limited creativity and computational decoupling in temperature-varied llm outputs of structured fictional data. *arXiv preprint arXiv:2502.08515* (2025).
10. Aoyama, T. & Wilcox, E. Language models grow less humanlike beyond phase transition. *arXiv preprint arXiv:2502.18802* (2025).
11. Porter, B. & Machery, E. Ai-generated poetry is indistinguishable from human-written poetry and is rated more favorably. *Sci. Reports* **14**, 26133 (2024).
12. Kovács, B. The turing test of online reviews: Can we tell the difference between human-written and gpt-4-written online reviews? *Mark. Lett.* **35**, 651–666 (2024).
13. Becker, S., Zhang, Y. & Lee, A. A. Geometry of energy landscapes and the optimizability of deep neural networks. *Phys. review letters* **124**, 108301 (2020).
14. Draxler, F., Veschgini, K., Salmhofer, M. & Hamprecht, F. Essentially no barriers in neural network energy landscape. In *International conference on machine learning*, 1309–1318 (PMLR, 2018).
15. Ballard, A. J. *et al.* Energy landscapes for machine learning. *Phys. Chem. Chem. Phys.* **19**, 12585–12603 (2017).
16. Bovier, A. *Statistical mechanics of disordered systems: a mathematical perspective*, vol. 18 (Cambridge University Press, 2006).
17. Auffinger, A., Arous, G. B. & Černý, J. Random matrices and complexity of spin glasses. *Commun. on Pure Appl. Math.* **66**, 165–201 (2013).
18. Nguyen, M. *et al.* Turning up the heat: Min-p sampling for creative and coherent llm outputs. *arXiv preprint arXiv:2407.01082* (2024).
19. Panchenko, D. The sherrington-kirkpatrick model: an overview. *J. Stat. Phys.* **149**, 362–383 (2012).
20. Bates, E. & Sohn, Y. Crisanti-Sommers formula and simultaneous symmetry breaking in multi-species spherical spin glasses. *Comm. Math. Phys.* **394**, 1101–1152 (2022).
21. Pavlopoulos, G. A. *et al.* Bipartite graphs in systems biology and medicine: a survey of methods and applications. *GigaScience* **7**, giy014 (2018).
22. He, X., Gao, M., Kan, M.-Y. & Wang, D. Birank: Towards ranking on bipartite graphs. *IEEE Transactions on Knowl. Data Eng.* **29**, 57–71 (2016).
23. Saadat, M., Khan, M. H., Ullah, N. & Asad, M. Impact of ai on language evolution: Analyze how ai tools like chatgpt are influencing language use, slang and new linguistic trends in digital spaces. *Policy Res. J.* **2**, 1819–1823 (2024).
24. Bender, E. M. & Koller, A. Climbing towards NLU: On meaning, form, and understanding in the age of data. In Jurafsky, D., Chai, J., Schluter, N. & Tetreault, J. (eds.) *Proceedings of the 58th Annual Meeting of the Association for Computational Linguistics*, 5185–5198, DOI: [10.18653/v1/2020.acl-main.463](https://doi.org/10.18653/v1/2020.acl-main.463) (Association for Computational Linguistics, Online, 2020).
25. Walsh, M. Tf-idf with scikit-learn.
26. Villani, C. & Villani, C. The wasserstein distances. *Optim. transport: old new* 93–111 (2009).

27. Piccoli, B. & Rossi, F. On properties of the generalized wasserstein distance. *Arch. for Ration. Mech. Analysis* **222**, 1339–1365 (2016).
28. Beckman, E., Cho, H. & Huynh, L. Inferring birth versus death dynamics for ecological interactions in stochastic heterogeneous populations. *arXiv preprint arXiv:2410.09041* (2024).
29. Bates, E., Sloman, L. & Sohn, Y. Replica symmetry breaking in multi-species sherrington–kirkpatrick model. *J. Stat. Phys.* **174**, 333–350 (2019).
30. Collins-Woodfin, E. W. & Le, H. G. Free energy fluctuations of the bipartite spherical sk model at critical temperature. In *Annales Henri Poincaré*, 1–61 (Springer, 2024).
31. Collins-Woodfin, E. & Le, H. G. Order of fluctuations of the free energy in the positive semi-definite msk model at critical temperature. *arXiv preprint arXiv:2501.11732* (2025).

## Acknowledgments

We are thankful to Professor Dimitrios Giannakis for his help with paperwork for the Committee for the Protection of Human Subjects (CPHS) and Undergraduate Research Assistantships at Dartmouth (URAD), ChatGPT for coding assistance, the anonymous individuals who filled out our survey, Undergraduate Advising and Research (UGAR) for funding, and the Institute for Computational and Experimental Research in Mathematics (ICERM) for the opportunity to present our work and providing travel support.

## Author contributions statement

L.H. designs and supervises the project. All authors discussed ideas, collected data, wrote code, produced figures, and wrote the main manuscript.

## Additional information

**Data collection:** All authors completed the Collaborative Institutional Training Initiative (CITI) Human Research course prior to conducting any research with human subjects.

### Data and code availability:

<https://github.com/lhuynhm/LLMs-probability-socialnetworks-language>

**Competing interests** The authors declare no competing interests.